Volume 3
Number 8
21 April 2021
Pages 2107–2386

Nanoscale Advances

rsc.li/nanoscale-advances

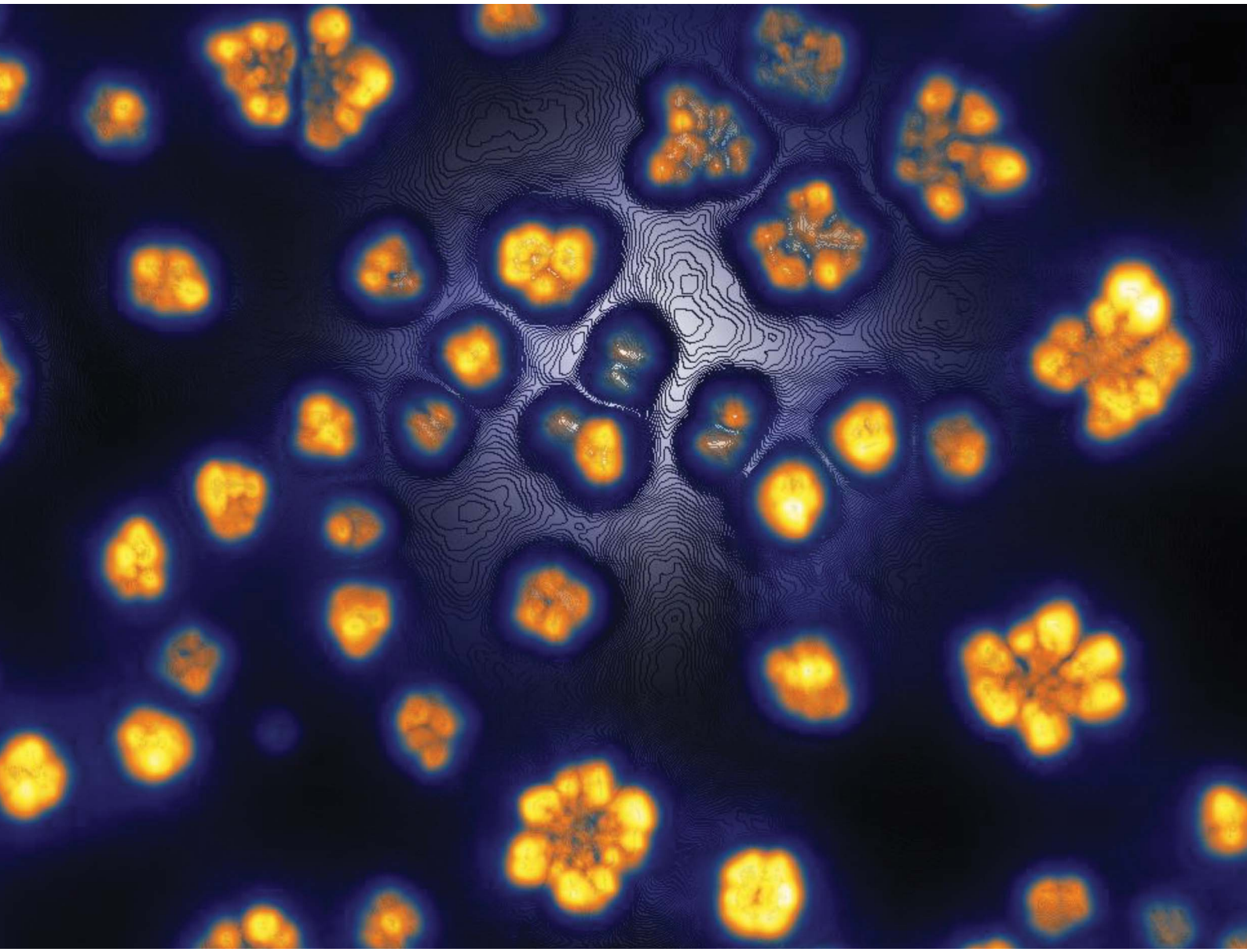

ISSN 2516-0230

ROYAL SOCIETY OF CHEMISTRY

PAPER

Yingqiu Xie *et al.*

Generation of particle assemblies mimicking enzymatic activity by processing of herbal food: the case of rhizoma polygonati and other natural ingredients in traditional Chinese medicine

NCNST

Nanoscale Advances

ROYAL SOCIETY OF CHEMISTRY

PAPER

View Article Online
View Journal | View Issue

Check for updates

Cite this: *Nanoscale Adv.*, 2021, **3**, 2222

Generation of particle assemblies mimicking enzymatic activity by processing of herbal food: the case of rhizoma polygonati and other natural ingredients in traditional Chinese medicine†

Enrico Benassi,‡[a] Haiyan Fan, ‡[b] Qinglei Sun,‡[c] Kanat Dukenbayev, ‡[d] Qian Wang,§[e] Ainur Shaimoldina,§[b] Aigerim Tassanbiyeva,[b] Lazzat Nurtay,[b] Ayan Nurkesh,[b] Aidana Kutzhanova,[b] Chenglin Mu,[f] Adilet Dautov,[b] Madina Razbekova,[b] Anar Kabylda,[b] Qing Yang,[b] Ziye Li,[g] Amr Amin,[hi] Xugang Li[f] and Yingqiu Xie *[b]

Processed herbs have been widely used in eastern and western medicine; however, the mechanism of their medicinal effects has not yet been revealed. It is commonly believed that a central role is played by chemically active molecules produced by the herbs' metabolism. In this work, processed rhizoma polygonati (RP) and other herbal foods are shown to exhibit intrinsic phosphatase-like (PL) activity bounded with the formation of nano-size flower-shaped assembly. *Via* quantum mechanical calculations, an enzymatic mechanism is proposed. The enzymatic activity may be induced by the interaction between the sugar molecules distributed on the surface of the nanoassemblies and the phosphatase substrate *via* either a hydroxyl group or the deprotonated hydroxyl group. Meanwhile, the investigation was further extended by processing some fresh herbs and herbal food through a similar protocol, wherein other enzymatic activities (such as protease, and amylase) were observed. The PL activity exhibited by the processed natural herbs was found to be able to effectively inhibit cancer cell growth *via* phosphatase signaling, possibly by crosstalk with kinase signaling or DNA damage by either directly binding or unwinding of DNA, as evidenced by high-resolution atomic-force microscopy (HR-AFM). In this work, the neologism herbzyme (herb + enzyme) is proposed. This study represents the first case of scientific literature introducing this new term. Besides the well-known pharmacological properties of the natural molecules contained in herbs and herbal food, there exists an enzymatic/co-enzymatic activity attributed to the nanosized assemblies.

Received 16th November 2020
Accepted 8th January 2021

DOI: 10.1039/d0na00958j

rsc.li/nanoscale-advances

Open Access Article. Published on 13 January 2021. Downloaded on 12/5/2025 2:40:49 AM.
This article is licensed under a Creative Commons Attribution-NonCommercial 3.0 Unported Licence.

Introduction

Herbs have been one of the pillars of medicinal practice for thousands of years. In "*An Outline Treatise of Medical Herbs*", compiled by Li Shizhen in 1596 (Ming Dynasty; Nanjing, China) and translated and published in Milan (Italy) in 1676,[1] over 1892 different species of herbs are quoted. In Traditional Chinese Medicine (TCM), and in particular Chinese herbology, Pao Zhi is a processing technique aimed at altering the properties, sterilizing and removing poisons from crude herbs by utilizing heat or other methods. In details, it may involve washing, soaking, boiling, steaming, fermenting, drying, roasting, frying, calcining, or other means.[2] This is a kind of alchemical processing used in the everyday preparation of herbal medicines, mineral and animal medicines, in TCM; it remains mysterious in terms of processing conditions, such as the type of container

[a]*School of Chemistry and Chemical Engineering, Shihezi University, Shihezi 832003, P. R. China*

[b]*School of Sciences and Humanities, Nazarbayev University, 53 Kabanbay Batyr Ave, Nur-Sultan, 010000, Republic of Kazakhstan. E-mail: yingqiu.xie@nu.edu.kz; xieautumnus@yahoo.com; Tel: +7 7172 694686*

[c]*Key Laboratory for Applied Technology of Sophisticated Analytical Instrument of Shandong Province, Shandong Analysis and Test Center, Qilu University of Technology (Shandong Academy of Sciences), Jinan, China*

[d]*School of Engineering and Digital Sciences, Nazarbayev University, Nur-Sultan, 010000, Republic of Kazakhstan*

[e]*Tai'an Xianlu Food Co Ltd, Tai'an, China*

[f]*Sino-German Joint Research Center on Agricultural Biology, State Key Laboratory of Crop Biology, College of Life Sciences, Shandong Agricultural University, Tai'an, 271018, China*

[g]*Huarun Taian Pharmacy Co. Ltd., Tai'an, China*

[h]*Biology Department, United Arab Emirates University, Al Ain 15551, United Arab Emirates*

[i]*The College, The University of Chicago, Chicago, IL 60637, USA*

† Electronic supplementary information (ESI) available. See DOI: 10.1039/d0na00958j

‡ Co-first authors.

§ Contributed equally.

© 2021 The Author(s). Published by the Royal Society of Chemistry

Open Access Article. Published on 13 January 2021. Downloaded on 12/5/2025 2:40:49 AM. This article is licensed under a Creative Commons Attribution-NonCommercial 3.0 Unported Licence.

(ceramic, clay, metal, …) or solvent used and the processing time. Despite its many unclarified aspects and unscientific approach, Pao Zhi is acknowledged as being effective at producing treatments for a wide variety of diseases; for example, in recent times, herbs were even found to be useful in combating the coronavirus SARS-CoV-2.

From a biochemical perspective, such processing would quickly denature the protein, and therefore no enzymatic activity would be expected. Taking advantage of modern scientific approaches, some studies have evidenced that a particular herb or a unique combination of different kinds of herbs as used in TCM exhibit antibacterial and anticancer functions, and about a third of cancer patients have accepted herbal medicine at certain stages of their treatment.[3,4] To date, the anticancer mechanism of TCM is proposed as inhibiting tumor angiogenesis, in the immune system, cell energy metabolism, cell cycle arrest, proliferative signaling, inflammation, and metastasis, which eventually cause cancer cell death or the reduction of chemotherapy toxicity.[5,6] It is commonly believed in the scientific literature that the specific chemical components contained in herbs are responsible for effects such as antioxidant, oxidant, and anti-inflammation.[7] Sometimes, some specific functional groups carried by the chemical components in TCM exert anticancer effects through regulation of the pH, ionic strength, redox activity, and many other chemical and physical characteristics within the biological environment.[8] So far, the anticancer and antimicrobial effects of TCM have never been attributed to any enzyme-like mechanism.

The anticancer or antimicrobial effects of herbs used in TCM have been attributed to the chemical components and functional groups, and the processing protocols and the processing protocols take relevant roles to different degree. However, in the in the hundreds of years practice of TCM, herb processing is not detached from herb choice and plays an equally vital role in curing a specific disease. As a matter of fact, the processing procedures for different herbs have been recorded in detail in ancient TCM books. According to the World Health Organization, processing methods – including boiling, steaming, roasting, stir-frying, baking, drying, sun-drying, shade-drying or thermo-drying – have the primary functions of neutralization of toxicity, reduction of side effects, and reinforcement of therapeutic efficiency.[9] Some previous studies indicate that processing and, in particular, curing, may induce some chemical reactions that affect the pH or redox properties, and therefore alter the biological functions.[10–12] Using mass spectrometry, Su *et al.* pointed out that different combinations of six compounds with varying percentages of each were obtained by adjusting the drying conditions in the processing of *Notopterygium franchetii*.[13] However, the impact of processing on the physical and chemical properties of herb-based TCM has not been systematically studied yet.

Other than processing, the medicinal effects of TCM are highly dependent on the environment where the herbs grow, as the chemical components, pH, and other chemical and physical properties of herbs significantly depend on the climate, soil, humidity, and other environmental factors. Rhizoma polygonati (RP, or Huang Jing), for instance, has been cultivated for thousands of years in various locations in China with their own particular climates and soil compositions. Originally recorded in Tao Hong Jing's "*Ming Yi Bei Lu*" (a Miscellaneous Records of Famous Physicians, dated 510 CE, Han Dynasty), RP is included in the *Pharmacopoeia of the People's Republic of China*[14] and its usage in TCM practice is becoming increasingly popular. RP's unique properties were commended in *Zhang Ren Shan* by Tang Dynasty poet Du Fu (712–770), who noted how RP "may renew the white hair with black, keep countenance the same through ice and snow."[15] In "*Compendium of Materia Medica*",[1] RP is acknowledged to supplement deficiencies, nourishment, and replenish "*qi* and blood".[16] Active components in RP, such as steroidal saponins, homoisoflavanones, lectins, polysaccharides, and alkaloids, along with crude methanol or water extracts, exhibit anticancer activity *in vitro* and *in vivo* through enhancement of the immune system and intervening in the apoptosis or autophagy signaling of cancer cells.[5]

Concerning RP processing, the earliest record was in "*Qian Jin Yao Fang*" (Tang Dynasty, Sun, Simiao),[17] wherein the treatment of RP requires steaming nine times and sun-drying nine times to achieve a better taste, along with more potent pharmaceutical effects with reduced toxicity.[5] Nevertheless, the connection between herb processing and enhanced treatment effectiveness remains elusive. Herein, we attempted to study the effects of processing of RP on the morphology and the formation of nanostructures, and how these may contribute to the enzymatic activities at the molecular level. The present work considers RP grown in the Mount Tai (RP Tai) area as a study case.

At the forefront of nanotechnology, nanozymes have recently been proposed as a novel concept.[18–20] As emerging artificial enzymes, metal-based and carbon-based nanozymes have been developed, representing two major classifications of nanozymes. The metal-based nanozymes are technologically more mature and exhibit peroxidase (POD),[18,21,22] oxidase (OD),[23] SOD,[24] and even PL activities,[25] whereas carbon-based nanozymes exhibit some POD activity.[26] Nanozymes with POD activity have been applied to the practice of antibacterial and anticancer therapy, mainly through the production of $^{\bullet}OH$ species by peroxidase.[27–29] Whether metal-based or not, nanozymes generally require specific regulated assembly, wherein some key functional groups form clusters with a repetitive pattern to ensure the enzymatic functioning. In our previous research, carbon nanodots developed from food or herbal food were shown to exhibit PL activity, and their binding to the phosphate group on the protein was identified by molecular spectroscopy and supported by quantum mechanical calculations.[30] Phosphatases, especially tyrosine phosphatase (PTP), have been recognized to suppress cancer cell growth and other oncogenic characteristics by intervening in cell signaling, wherein phosphatase most likely dysregulates the phosphorylation–dephosphorylation balance to disrupt cancer cell signaling.[31–33] As a continuation of our previous work, we aim to correlate the nanostructures or their assemblies formed through RP processing with the enzyme-like activities demonstrated in the final products by means of FT-IR spectroscopy and enzymatic tests combined with quantum mechanical calculations. A neologism is proposed here to summarise the

Open Access Article. Published on 13 January 2021. Downloaded on 12/5/2025 2:40:49 AM.
This article is licensed under a Creative Commons Attribution-NonCommercial 3.0 Unported Licence.

new concept of enzyme-like effects of processed herbs, *i.e.*, herbzyme, coming from the merging of herb and enzyme.

Results and discussion

Processing RP generates nanoparticles exhibiting PL activity: herbzyme

In this section, commercial RP Tai, which was processed according to the TCM protocol, was characterized and subjected to phosphatase enzymatic tests. The element analysis obtained by SEM-EDS (ESI Fig. S1†) indicates that, other than C, O, and H, there are significant amounts of Si, Cl and S, which are likely absorbed from the soil. The HR-AFM image of commercial RP in Fig. 1a shows some flower-shaped assemblies with dimensions of 200–500 nm × 200–500 nm × 50 nm. Such assemblies generally feature some "heads" lining a circle, leaving their "tails" pointing toward the center of the circle. Assemblies with rather similar patterns were observed in the SEM image in Fig. 1b. The structure of such assemblies is analogous to that of lipids, wherein the hydrophilic heads are arranged on the circle, whereas the hydrophobic tails are confined within the circle. Both HR-AFM and SEM images show some highly regulated nanostructure assemblies for the processed RP, whereas the AFM image for the fresh RP shows some particles with a spherical shape and much bigger average size (ESI Fig. S2†). Besides, for the fresh RP, such patterned morphology was absent.

After filtration using a syringe filter with a pore size of 200 nm, the aqueous solution of RP was separated into two parts, one containing the smaller sized particles (RP-nano) and one with bigger sized particles (RP-micro). Fluorescence centered at 460 nm and ~680 nm was observed for both the RP-nano and RP-micro solutions (Fig. 1c). The fluorescence of the former is nearly identical to that of most carbon-based nanodots with particle size below 10 nm,[34] whereas the latter has been rarely reported before. Consistently, the SEM image (ESI Fig. S3(a)†) for RP-nano exhibits some ring-shaped assemblies with an average diameter smaller than 100 nm. In contrast, the SEM image of RP-micro (ESI Fig. S3(b)†) shows a continuous aggregation of many smaller particles, and the aggregated feature has an average size larger than 1 μm.

Therefore, we hypothesize that the particles with bigger size are responsible for the fluorescence emission at 680 nm. Hence, both morphological and spectroscopical data confirm that the commercial RP contains a significant number of nanoparticles.

Upon filtration through a 200 nm filter, the RP-nano then underwent enzymatic screening, specifically, the phosphatase activity test, wherein nitro blue tetrazolium (NBT)/5-bromo-4-chloro-3-indolyl phosphate (BCIP) was used as the substrate. The phosphatase test showed positive result at pH 13 *in vitro*, at

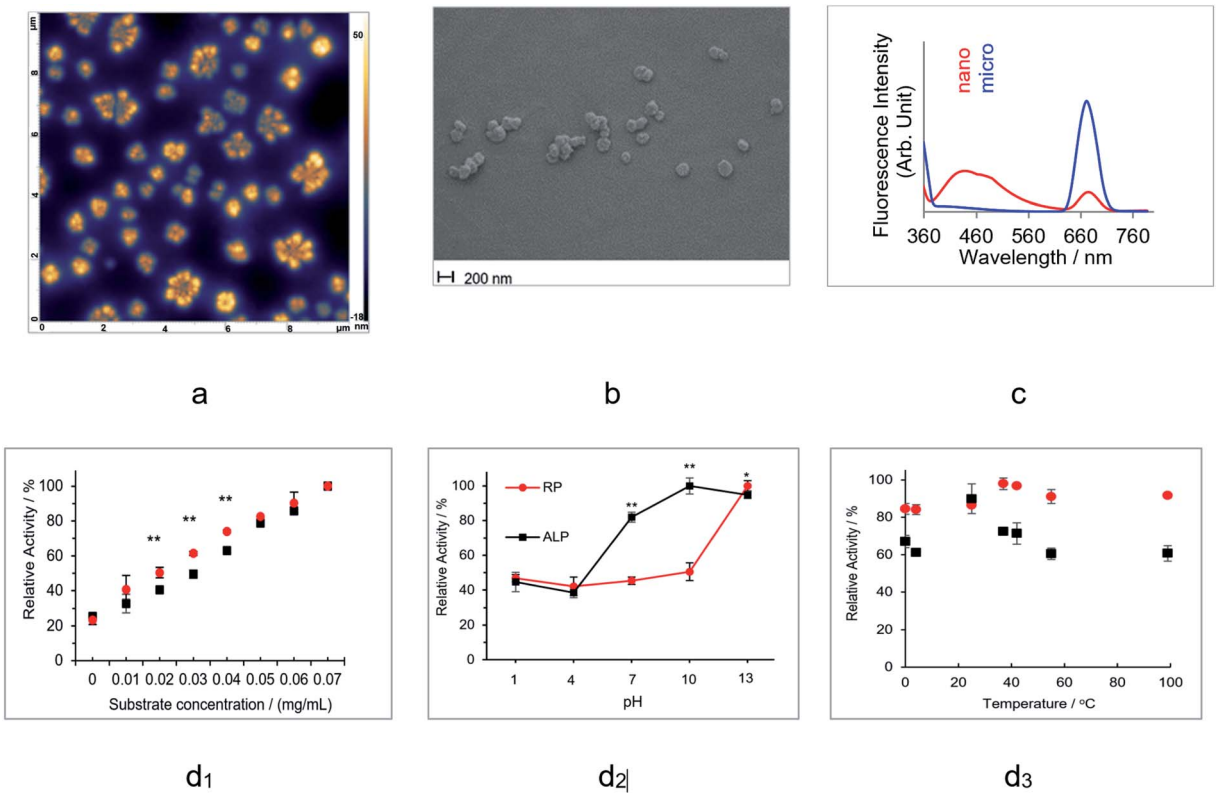

Fig. 1 Characterization of the processed RP and its interaction with DNA: (a) AFM image of RP Tai using the dried solution sample at a concentration of 50 mg mL^{-1}. (b) SEM image of RP Tai using the dried solution sample at a concentration of 50 mg mL^{-1}. (c) Fluorescence spectra of RP-nano and micro with an excitation wavelength of 350 nm. (d) Phosphatase tests for RP Tai and ALP with NBT/BCIP substrate: (d_1) substrate concentration dependence at pH 13; (d_2) pH dependence; and (d_3) temperature dependence at pH 13.

© 2021 The Author(s). Published by the Royal Society of Chemistry

Open Access Article. Published on 13 January 2021. Downloaded on 12/5/2025 2:40:49 AM.
This article is licensed under a Creative Commons Attribution-NonCommercial 3.0 Unported Licence.

which RP exhibits slightly more vigorous PL activity than that of the natural alkaline phosphatase (ALP) (Fig. 1d). The pH dependence tests indicate that ALP holds more robust phosphatase activity than RP in the pH range of 4 to 13, and the PL activity of RP catches up at pH 13. The temperature dependence tests indicated that RP maintained a stable PL activity from 0 °C to 99 °C, whereas ALP only reached the same activity as RP at 25 °C and exhibited significantly reduced activity at all other temperatures.

In summary, the PL activity of the processed RP was confirmed; owing to this pseudo-enzymatic activity, hereafter, we shall refer to the nanoassemblies contained in the processed herbs as RP herbzymes.

Nanoassemblies and their correlation with PL activity observed for processed herbs and herbal foods other than RP

A hypothesis is proposed hereby that the morphology of the herbal material highly depends on the processing. Baking generally produces a large amount of smaller sized particles, yet they are assembled with highly regular patterns; successful examples were obtained with extracts from *Zingiber officinale* and *Lycium chinense*. The AFM images show that the surface morphology of the fresh extract of *Zingiber officinale* (Fig. 2a) is in a random pattern with an average particle size of 50–100 nm × 50–100 nm × 50 nm; the fresh extract from *Lycium chinense* (Fig. 2b) exhibits a triangular pattern with dimensions of 1 μm

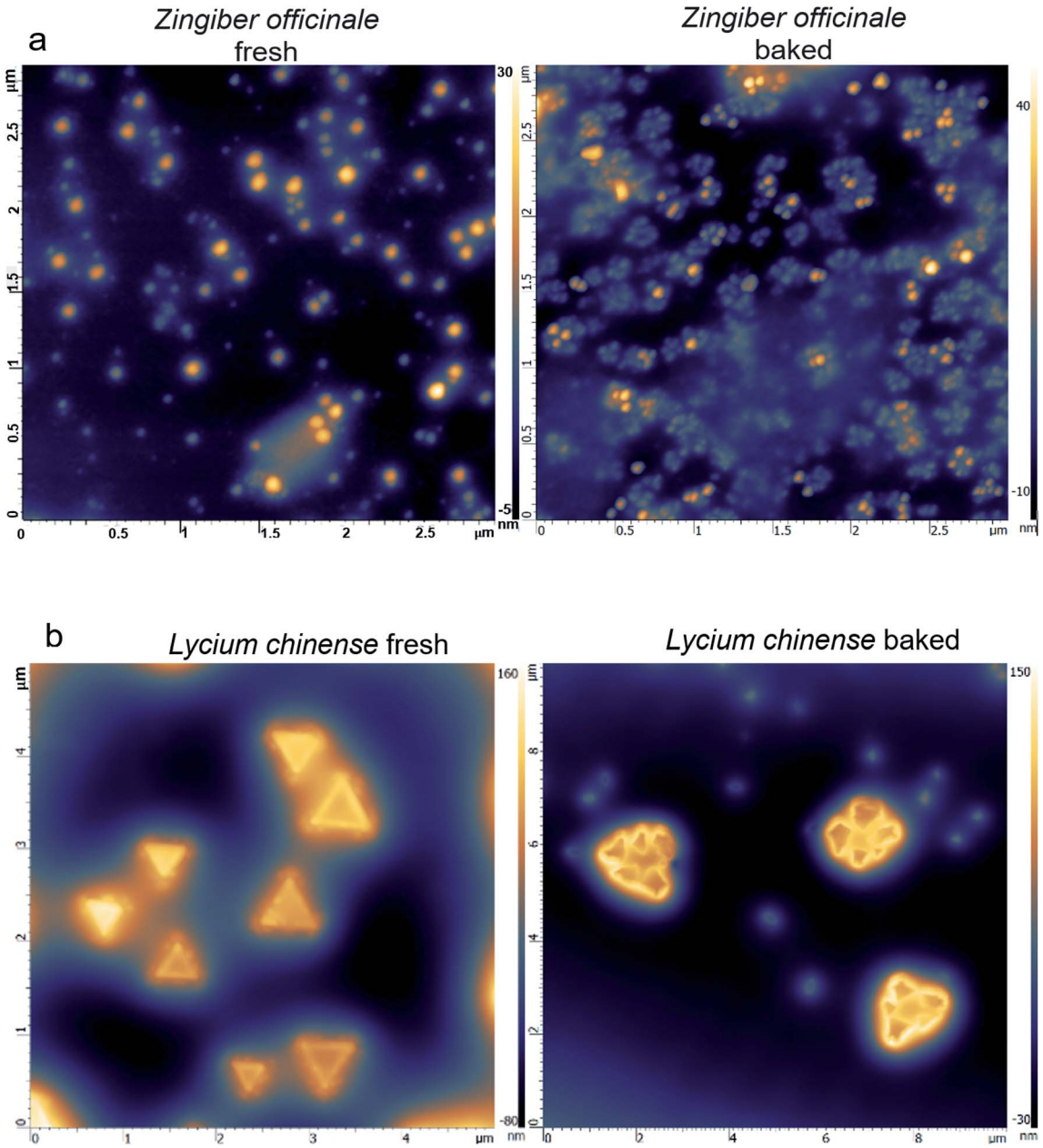

Fig. 2 Characterization of processed herbs followed by characterization of the hydrophobic components: (a) left panel: AFM image of fresh *Zingiber officinale*; right panel: AFM image of baked *Zingiber officinale*. (b) Left panel: AFM image of fresh *Lycium chinense*; right panel: AFM image of baked *Lycium chinense*.

Open Access Article. Published on 13 January 2021. Downloaded on 12/5/2025 2:40:49 AM. This article is licensed under a Creative Commons Attribution-NonCommercial 3.0 Unported Licence.

× 1 μm × 150 nm. Upon baking, the *Zingiber officinale* extract develops highly regulated flower-shaped assemblies and the *Lycium chinense* extract develops a pattern that is made of 4–6 smaller sized triangular assembles. In both cases, the average particle size significantly decreased.

On the other hand, PL activity is assumed to be closely correlated with the total amount of nanosized particles. Using an NBT–BCIP substrate, the PL activity of four species, *i.e.*, RP, *Lycium chinense*, *Allium schoenoprasum,* and *Zingiber officinale* (Fig. 3), was tested fresh and upon baking. Without exception, relatively enhanced PL activity was observed for the baked samples, which is mainly owing to the increase in the amount of nanosized particles upon baking. In a separate set of tests, the PL activity was compared between the fresh and baked samples for 33 herbs or herbal vegetables (ESI Fig. S4†). Once again, 25 out of 33 species exhibited stronger PL activity for the baked samples than the fresh ones. We then conclude that the herb-zymatic activity is linked to the baking process.

The mechanism of processing-generated PL activity

The active centers of ALP and PTP were identified as two Zn^{2+} ions and the S–H functional group on cysteine, respectively; sometimes, in PTP the N–H group may cooperate with the dephosphorylation process.[35–38] A regular phosphatase protein inhibitor (PPi) did not act on RP-nano; on the contrary, it even enhanced the PL activity of RP in some circumstances. Three potential inhibitors were therefore applied to figure out the PL mechanism of RP. Elemental and amino acid analyses indicated that RP Tai contains outstanding levels of Ca^{2+} ions and glutamic acid (Glu) (quality report of the product). However, neither of these components are responsible for the reported phosphatase mechanism (Fig. 3b). While Ca^{2+} evidently inhibited ALP (Fig. 3b), it enhanced the PL activity of RP without showing concentration dependence in the range from 0.25 M to 2 M. Such observations imply that the PL activity brought by RP is different from that of ALP. On the other hand, EDTA exhibited a specific inhibition effect. However, with its pK_a values of 0, 1.5, 2, and 2.66, EDTA may easily lead to a pH variation in the medium, and it also holds tremendous potential to coordinate with the metal components in RP that might otherwise cause PL activity.

The effect of Na_2CO_3, Na_2SO_4, and $NaHCO_3$ on the phosphatase-like activity of RP was tested (ESI Fig. S5†). While Na_2CO_3 exhibited the least impact, both Na_2SO_4 and $NaHCO_3$ inhibited the PL activity of RP. Na_2SO_4 is a well-known dehydration reagent; its addition may cause the removal of some water molecules distributed on the surface of RP particles, which is perhaps quite relevant to the dephosphorylation, whereas the inhibition brought by $NaHCO_3$ is likely due to the pH variation.

To model the chemical mechanism of the PL activity of RP, quantum mechanical calculations were performed at the density-functional theory (DFT) level. It has been well established that RP contains a large amount of carbohydrates,[39] which are responsible for the sweet taste of the RP tea. To

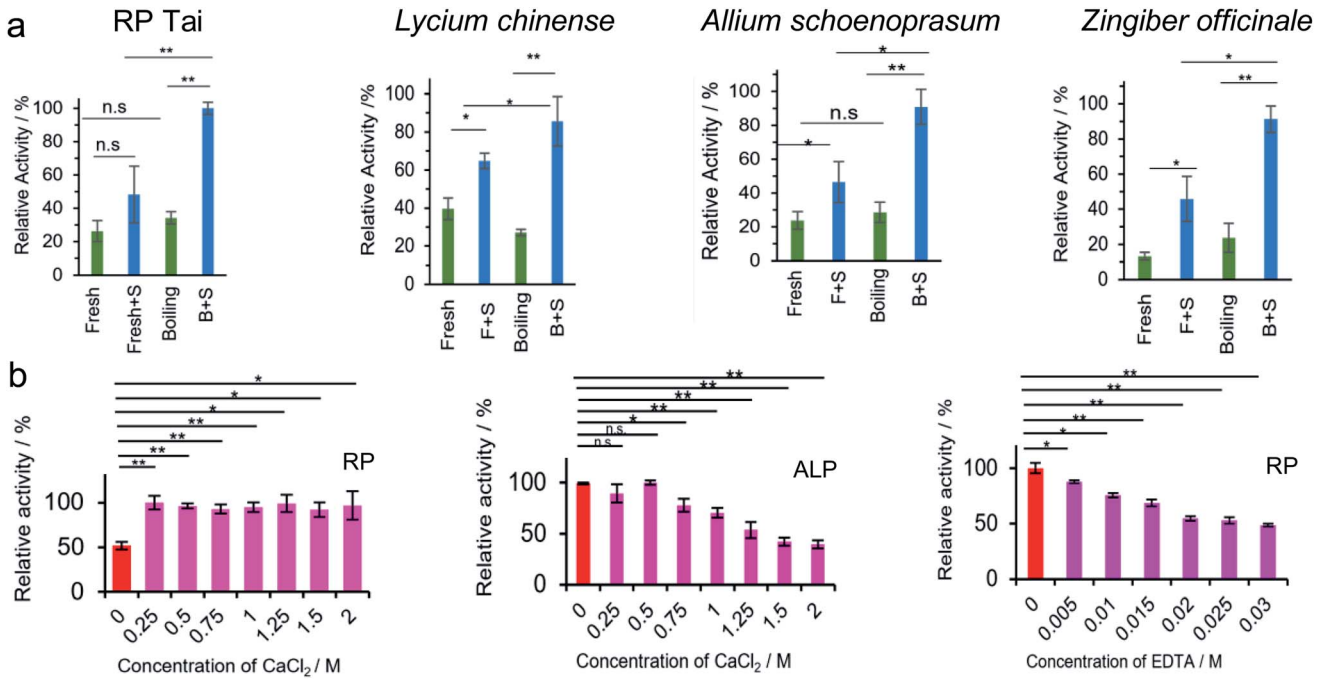

Fig. 3 (a) Characterization of herbs and herbal foods upon baking: PL activity test of RP Tai, *Lycium chinense*, *Zingiber officinale*, and *Allum schoenoprasum* with NBT/BCIP substrate at pH 13 (NBT/BCIP concentration: 0.15 mg mL^{-1}, herb concentration: 2.5 mg mL^{-1}). S represents substrate. (b) Phosphatase inhibition tests by Ca^{2+} and EDTA with NBT/BCIP substrate; left panel: inhibition tests by Ca^{2+} against RP; middle panel: inhibition tests by Ca^{2+} against ALP; right panel: inhibition tests by EDTA against RP. * = significant difference with $p < 0.05$; ** = significant difference with $p < 0.01$.

© 2021 The Author(s). Published by the Royal Society of Chemistry

Open Access Article. Published on 13 January 2021. Downloaded on 12/5/2025 2:40:49 AM.
This article is licensed under a Creative Commons Attribution-NonCommercial 3.0 Unported Licence.

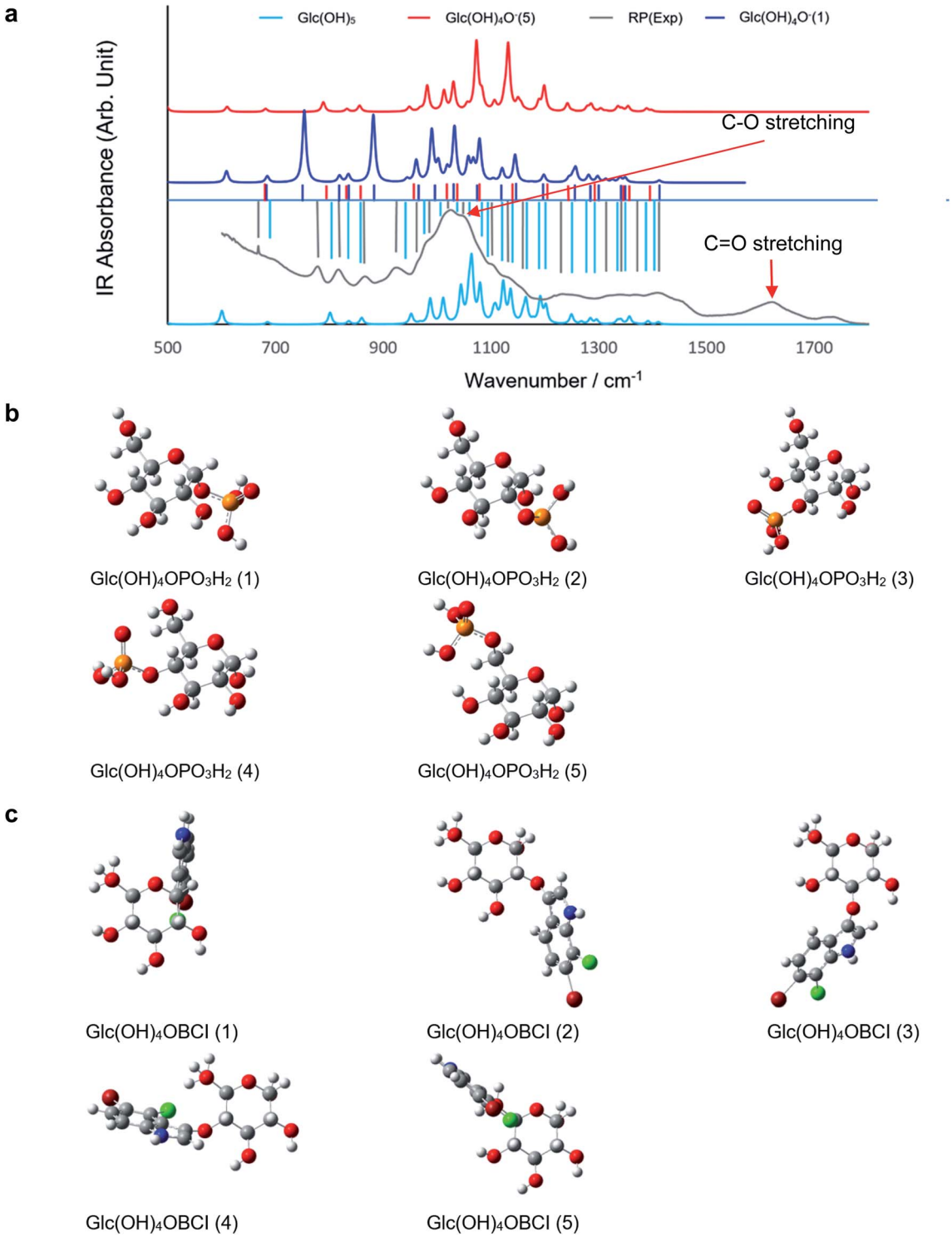

Fig. 4 Phosphatase mechanism study: (a) FT-IR spectrum of RP Tai; the calculated IR spectra of neutral glucose $Glc(OH)_5$ and glucose deprotonated at position 1 and 5 $Glc(OH)_4O^-$ (1)/(5). (b) The five isomeric molecular structures of the dimers formed between glucose and phosphate. (c) The five isomeric molecular structures of the dimers formed between neutral glucose and BClO.

efficiently model these compounds, only α-D-Glucose (Glc) was investigated as the most representative monosaccharide of RP. In particular, it is well-known that in aqueous solution both open-chain and cyclic forms are in equilibrium, but at pH 7 the cyclic one is predominant, and therefore in this investigation, only the cyclic structure of Glc was considered. The computational modeling consisted of studying the phosphate group exchange between BCIP and Glc. Glc is a polyol, bearing five hydroxyl groups; it is more acidic than simple alcohols with a pK_a of first deprotonation equal to 12.46 (ref. 40) (*e.g.*, methanol's $pK_a = 15.5$). Our calculations and the literature[41] support this experimental evidence. Deprotonation of an alcohol group

Open Access Article. Published on 13 January 2021. Downloaded on 12/5/2025 2:40:49 AM.
This article is licensed under a Creative Commons Attribution-NonCommercial 3.0 Unported Licence.

in Glc facilitates the cyclization reaction because the conjugate base (alkoxide) is a much stronger nucleophile.[42] We therefore suppose that the choice of the cyclic form is reasonable for our purposes. Considering the temperature and pressure adopted, the processing may not dramatically change the chemical structure and composition, although it may bring specific morphological changes and affect the charge distribution, as observed in the present study. The electrophoresis tests indicated significant amount of components in RP carry negative change, which may be attributed to deprotonated sugars. The experimental FT-IR spectrum of RP was compared with the calculated IR spectra of neutral Glc ($Glc(OH)_5$) along with the two isomers of the singly deprotonated Glc ($Glc(OH)_4O^-$), *viz.* in positions 1 and 5 (Fig. 4a). The experimental absorption bands match the calculated ones, especially for $Glc(OH)_4O^-$ (1), the most stable deprotonated isomer, suggesting that, after processing, RP may contain both neutral and deprotonated sugars.

Given the chemical nature of RP, the most likely candidate responsible for the negative charge should be the deprotonated carboxylic group considering its pK_a value of ~4.75. If this is the case, a dramatic frequency shift should be observed for C=O from fresh RP to processed RP as the C=O in the neutral carboxylic group is characterized by the IR absorbance centered at ~1720 cm^{-1}, whereas the C=O in the deprotonated carboxylic group should have IR absorption at ~1680 cm^{-1}. Such a peak shift was never observed in the present work; therefore, it is reasonable to assume that the deprotonated hydroxyl group on the sugar molecule is responsible for the negative charge after processing. Considering the results of the previous sections, we concluded that processing leads to the production of nanosized particles. When a molecule is in a form of nanoscaled assembly, its reactivity as well as stability usually indicate differences from the situation wherein the molecules are segregated by the solvent molecules. At the nanoscale it becomes possible for some species to exist that otherwise will be unstable to stay balanced among the specific surface tension, surface defects, and the interaction among the particles with similar dimensions. Anyway, the sudden enhancement of the PL activity observed at pH = 13 for RP provides another hint that the deprotonation of Glc is indeed realistic.

Concerning modeling a possible mechanism for RP's phosphatase-like activity, two possible competitive reaction paths may be hypothesized: (1) a protonated or deprotonated sugar molecule reacts with BCIP, and the phosphate group is transferred from the latter to the former *via* a transition state, to eventually obtain phosphorylated sugar (GlcP; Fig. 4b) and BCI (protonated in keto form, or deprotonated as enolate); or (2) the sugar molecule and BCIP dimerize together (forming Glc–O–BCI; Fig. 4c) with the release of the phosphate group. There are five possible isomers for GlcP and Glc–O–BCl. From the energetic perspective, both of the proposed paths are thermodynamically favored at n.c. ($\Delta G_{T,p} \ll 0$). However, among the isomers, GlcP (1) and (5) were the most abundant products of the sugar phosphorylation (11% and 84% at room temperature, respectively), whereas Glc–O–BCI (4) and (5) were the major products for the dimerization (40% and 59% at room temperature, respectively). Kinetic-wise, the lowest value of $\Delta G^{\ddagger}$ (4.8 kJ mol^{-1}) was identified for the phosphate group exchange wherein the –OH or RO^- group in position 1 acts as the dephosphorylation center; the corresponding transition state was characterized by triangular bipyramidal coordination of the P atom and two hydrogen-bonding interactions formed by the two –OH groups of the phosphate moiety and the ether oxygen (of Glc) and the alkoxy oxygen (of BCI) occupying one of the two apical positions of the P coordination shell.

Quantum mechanical calculations not only lay a strong foundation at the molecular level for the enzymatic activity but also emphasize the importance of molecular assembly, which plays a key role in terms of the arrangement of repetitively aligned clusters of key functional groups in a particular conformation. These are two critical aspects of the resulting enzymatic performance. Once again, it manifests the strong effect of herbal processing, which will be discussed in depth in the following sections.

The role of boiling in the PL activity

Boiling represents the most common processing practice adopted by TCM. It has been reported that thermal treatment of poly-sugars potentially generates aggregated mono-sugars, sugar oligomers, or dehydrated sugars, and consequently alters the molecular structure of the poly-sugars.[43–45] Herein, four common herbs, including *Leonurus artemisia*, *Panax quinquefolis*, *Gynostemma pentaphyllum*, and *Angelica sinensis*, were chosen to compare the PL activity between fresh and boiled samples. The impact of boiling was detected by fluorescence at 460 nm and 690 nm, which manifests the change in the amount of nano- and micro-sized particles, respectively, as well as the FT-IR absorbance centered at 1050 cm^{-1} corresponding to the C–O stretching vibration, which reflects the change in the distribution and orientation of the functional groups on the surface of the herbal particles (Fig. 5a–d). All four herbs showed more robust PL activity upon boiling. For *Leonurus artemisia*, the enhanced PL activity can be attributed to the increase in the number of nanosized particles and more exposed alkoxide functional groups on the surface of the particles. Without showing an increase in the fluorescence intensity at 460 nm, the promoted PL activity exhibited in boiled *Gynostemma pentaphyllum* is likely due to the molecular conformation change upon boiling that makes more functional groups available for the dephosphorylation. For *Panax quinquefolis*, boiling did not promote the production of nanosized herbal particles nor lead to an increase in the exposed alkoxide functional groups. Consequently, the boiled sample did not exhibit significantly improved PL activity. Finally, boiling had more impact on the exposure of the surface alkoxide groups than on the production of nanosized particles. Thus, the enhanced PL activity for the boiled samples is attributed to the increased number of exposed alkoxide groups on the surface of the herbal particles.

RP herbzymes can dephosphorylate DNA by PL activity thereby inducing DNA damage

Since ALP can dephosphorylate DNA at the 5′-phospho-end,[35] the RP herbzymes were applied to DNA 5′-phospho-end in

 © 2021 The Author(s). Published by the Royal Society of Chemistry

Open Access Article. Published on 13 January 2021. Downloaded on 12/5/2025 2:40:49 AM.
This article is licensed under a Creative Commons Attribution-NonCommercial 3.0 Unported Licence.

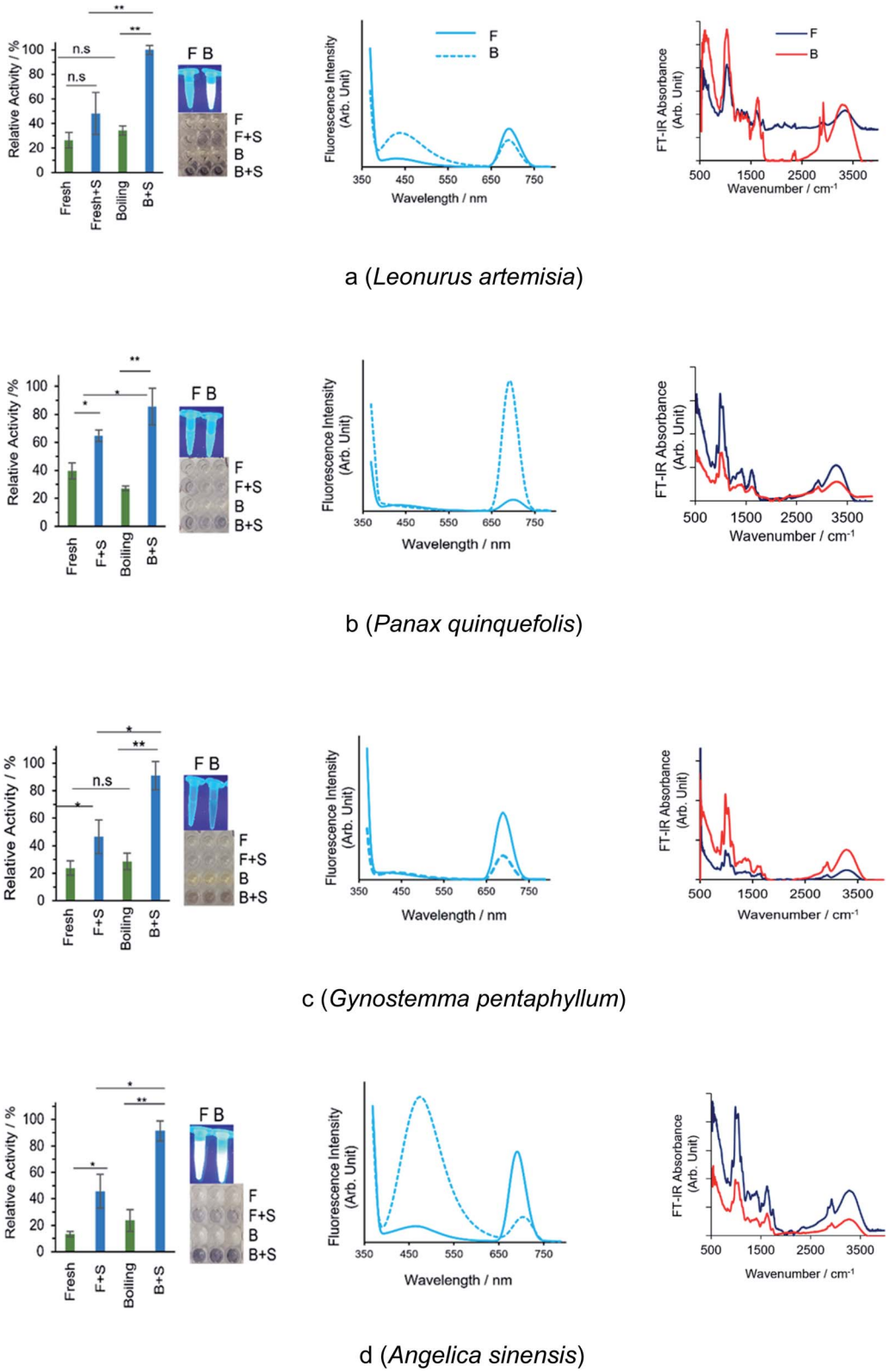

Fig. 5 Spectroscopic characterization and PL tests for the fresh (F) and boiled (B) herbs with the substrate (S): (a) *Leonurus artemisia*. Left panel: PL activity test for fresh and boiled herbs with NBT/BCIP as the substrate (S) at pH 13 (NBT/BCIP concentration: 0.15 mg mL^{-1}, herb concentration: 2.5 mg mL^{-1}). Middle panel: fluorescence spectra of fresh and boiled herb samples with an excitation wavelength of 350 nm. Right panel: FT-IR spectra of fresh and boiled herb samples (both dried). (b) *Panax quinquefolis*. (c) *Gynostemma pentaphyllum*; (d) *Angelica sinensis*. * = significant difference with $p < 0.05$; **significant difference with $p < 0.01$.

© 2021 The Author(s). Published by the Royal Society of Chemistry

Open Access Article. Published on 13 January 2021. Downloaded on 12/5/2025 2:40:49 AM.
This article is licensed under a Creative Commons Attribution-NonCommercial 3.0 Unported Licence.

electrophoresis tests. The dephosphorylation is evidenced in Fig. 6a for the ALP–DNA 5′-phospho-end system, wherein a new band likely representing 5′-dephospho DNA appeared. The same band distribution was observed for the RP herbzyme–DNA 5′-phospho-end system, confirming the dephosphorylation ability of the RP herbzymes. Other than the function of dephosphorylation, the RP herbzymes were found to establish a strong interaction with DNA, especially the RP with smaller particle size. Such interaction was observed using coiled plasmid DNA through HR-AFM. The flower-shaped RP particles with XY dimensions of 200–400 nm × 200–400 nm exhibited little affinity with coiled DNA (Fig. 6b), whereas the particles with an average size smaller than 50 nm show a stronger interaction with DNA, and some even caused the fragmentation of DNA, as indicated within the red circle in Fig. 6c and ESI Fig. S6.†

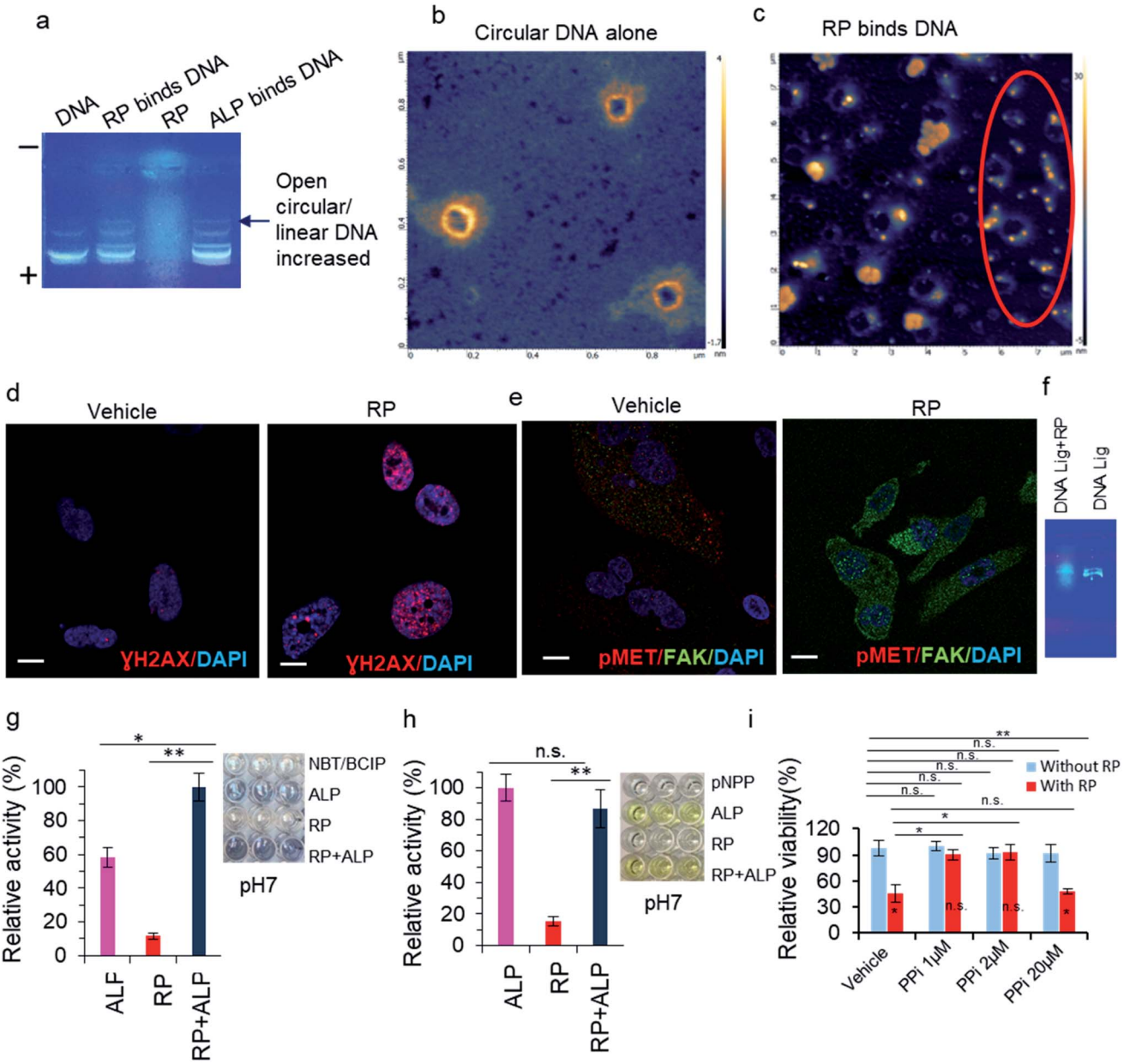

Fig. 6 RP binds DNA, induces DNA damage, regulates DNA ligation, and enhances phosphatase activity, thereby inhibiting cell growth: (a) agarose gel electrophoresis with DNA–RP system. (b) AFM images of DNA with the coiled shape (control). (c) AFM images of coil-shaped DNA after application of RP Tai solution of 50 mg mL^{-1}. (d and e) Confocal microscopic images of RP induce DNA damage, decreased phosphorylation of MET (pMET) and increased FAK in PC3 cells. (f) Agarose gel electrophoresis with RP effect on DNA ligation. (g) PL activity of RP + ALP with NBT/BCIP substrate at pH 7 (NBT/BCIP concentration: 0.15 mg mL^{-1}, herb concentration: 2.5 mg mL^{-1}, ALP: 1 : 50 000). (h) PL activity of RP + ALP with pNPP substrate at pH 7 (pNPP concentration: 5 mM, herb concentration: 2.5 mg mL^{-1}, ALP: 1 : 50 000). (i) Cell growth inhibition assay in 24 well plate by staining of cells by crystal violet. Phosphatase inhibitor (PPi) was used at concentration indicated. Scale bars: 20 μm. "*" means significant difference with $p < 0.05$, whereas "**" means significant difference with $p < 0.01$. "n.s." means non-significant.

© 2021 The Author(s). Published by the Royal Society of Chemistry

Open Access Article. Published on 13 January 2021. Downloaded on 12/5/2025 2:40:49 AM.
This article is licensed under a Creative Commons Attribution-NonCommercial 3.0 Unported Licence.

RP herbzyme-induced DNA damage during cell growth related to PL activity

As a readout of DNA binding and unwinding, the DNA damage induced by the herbzymes was identified in PC3 cancer cells detected by DNA damage marker staining, *via* gamma H2AX foci formation testing experiment with antibody staining (Fig. 6d and e). The DNA damage induced by the RP herbzymes is likely to be due to the herbzymes interfering in the ligation stages (Fig. 6f).

Moreover, the cell focal adhesion marker FAK increased and phosphor–MET decreased upon the RP treatment, suggesting that the role of RP is closely related to the FAK adhesion signaling and that RP decreases MET kinase phosphorylation (pMET) (Fig. 6e). Thus, the RP most likely acts as a phosphatase to inhibit MET kinase phosphorylation.

Finally, we tested whether the RP herbzymes can act through phosphatase *in vitro*, especially at pH 7, the physiological condition. The phosphatase substrates NBT/BCIP and pNPP were then applied to a combination of ALP and RP. As shown in Fig. 6, RP also intervenes in the cell signaling pathways through a selective regulation of phosphatase as RP promotes phosphatase activity with the NBT/BCIP substrate but not the pNPP substrate (Fig. 6g and h).

As one of the functions of phosphatase in cancer is tumor suppression, we further explored the potential application of the herbzymes for cancer cell growth inhibition. Phosphatase is known for its ability to prevent cell growth through the inhibition of kinase signaling. Hence more tests were performed to identify whether the RP–PL herbzymes inhibit cancer cell growth *via* crosstalk with phosphatase-induced kinase inhibition signaling. In cancer cells, when phosphatase was inhibited by sodium orthovanadate (SOV), an inhibitor of phosphatase (PPi), at 20 μM mL^{-1}, RP-mediated inhibition of cell growth at low dose is invalid (Fig. 6i). In other words, when the cell's endogenous phosphatase is blocked by PPi, RP lost the function of inhibiting cell growth. In more detail, when the cell's endogenous phosphatase is inhibited by PPi, RP did not inhibit cell growth. This suggests that the RP herbzymes inhibit cancer cell growth at least through phosphatase interaction-induced activity, which is consistent with the *in vitro* data in Fig. 6g and h.

In summary, processed herbs such as RP with nanostructures or highly regulated assemblies (*i.e.*, nanoflower-like structures) exhibited not only the full PL activity but also the ability to bind DNA, which interferes in DNA repair and causes cell death by targeting phosphorylation events.

Processed RP-nano exhibits enzyme activities other than PL

The RP herbzymes also demonstrated trypsin activity to digest proteins and α-amylase activity to digest starch (Fig. 7a and b). Thus, the processed RP-nano may have the potential for multiple enzyme activities. α-Amylase and trypsin are important enzymes in digestive systems that catalyze the hydrolysis of starch molecules to glucose to increase blood sugar levels and digest protein by cutting peptide bonds, respectively. They are essential in the food industry and biomedical physiological

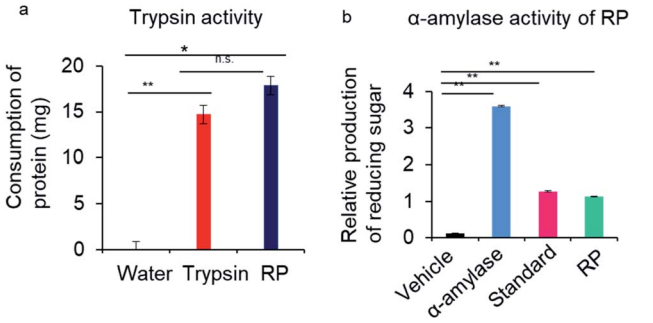

Fig. 7 Tests of enzymatic activities other than PL of RP herbzymes. (a) Trypsin activity of RP. (b) α-Amylase activity of RP. Standard solution refers to glucose, a reaction product. * = significant difference with $p < 0.05$; ** = significant difference with $p < 0.01$.

digestion. RP herbzymes can be potentially applied to gastric digestion in medical treatment,[6,48] especially through enhancing ALP at pH 7 or 8. In ancient records, processed RP is beneficial for digestion, but the mechanism had not been revealed until now. Here, we explained the biochemical enzyme activity induced by the herbzymes at the nanoscale, which provides the biochemical effect of the processed RP herbzymes .[6,47] This finding expands our understanding of the herb's enzyme activity at the nanoscale based on biophysical principles. Importantly, our findings expand nanozymes to include herbzymes generated by the processing of natural products, in addition to artificially synthesised or metal-based nanozymes.

Conclusions

Herb processing in TCM has been shown to generate nanosized particles and highly regulated assemblies that demonstrate PL or other enzymatic activities. This is the first report to reveal the critical role played by processing in TCM efficacy. Some inhibition tests indicated that the PL activity exhibited by the processed RP involved a different mechanism from that of ALP. Quantum mechanical simulation showed that the PL activity of the processed RP is achieved through the interaction between sugar molecules, particularly the deprotonated hydroxide functional groups, and the phosphate substrate.

On the other hand, cancer cells were sensitive to RP in cell spreading which is linked to FAK, MET signaling, being stem cells anchorage-independent cell growth. Moreover, phosphatase is acknowledged as a stem cell marker.[46] Therefore, further interesting studies would be functions of RP as artificial phosphatase herbzyme in stem cells or cancer stem cells.

Herbs and herbal foods other than RP were subjected to the tests in the present work and showed effective enzymatic or co-enzymatic activities, indicating that processing (baking or boiling) generally leads to the production of smaller particles on the nanoscale with highly regulated assemblies. These nanosized particles and their assemblies were found to play critical roles in the enzymatic properties reflected in

Open Access Article. Published on 13 January 2021. Downloaded on 12/5/2025 2:40:49 AM.
This article is licensed under a Creative Commons Attribution-NonCommercial 3.0 Unported Licence.

these processed herbs, therefore hinting that the medicinal effects of TCM are not only triggered by its chemical components, but also the processing, Pao Zhi, responsible for the assembly generation. The discovery in the present work may just be the tip of an iceberg of the secrets in the history of TCM practice. Further effort is needed to shed light on the thermodynamics and kinetics of the generation of the nanostructures and their assembly mechanism and the way the processing conditions (temperature, heating/cooling rates, *etc.*) influencd the size (and subsequently the effectiveness) of the processed herbs.

Finally, the present work provides a molecular model for the enzymatic features reflected in the processed herbs through quantum mechanical calculations. Meanwhile, it enriches the practice of generating nanozymes by introducing TCM processing methods. Above all, the present work broadens our insights into the principles of nanozymatic functions and expands our vision to explore the broader application of nanozymes, herbzymes in this particular case, through natural products at the nanoscale.

Materials and methods

Processing of herbs

The preparation and processing of the filiform of RP includes the following steps. Owing to patent policy, some steps are described in brief. Firstly, fresh RP root was thoroughly cleaned and cut into shreds. Secondly, the RP was further processed to become filiform slices of uniform filamentous shape with a cross-section size of 0.5–20 mm (the maximum length of the cross-section), with total saponin content of 3.32–3.54 mg/100 mg, and total flavonoids content of 4.23–4.79 mg g^{-1}. For the other herbs or herbal foods, 200 °C was used for baking and 100 °C for boiling for different lengths of time, as indicated in the figures or legends.

High-resolution atomic-force (HR-AFM), scanning electron (SEM) and confocal microscopy

High-resolution atomic-force microscopy imaging (HR-AFM) was performed using an AFM Smart SPM 1000 (AIST-NT, Russia). The scanning speed is 0.2 Hz. Pixel resolution is 1024 × 1024. Super sharp type NSG30_SS (NT-MDT Spectrum Instruments, Russia) cantilevers with tip radius curvature of 2 nm and resonance frequency of 200–440 kHz were applied for imaging in AC mode (tapping mode).

For the scanning electron microscopy images (SEM), the samples were air-dried, followed by SEM scanning of different fields. For confocal microscopy (LSM780, Carl Zeiss) analysis, the cells were plated on glass coverslips (Fisher) and treated with vehicle or herb extracts after 24 h. Finally, the cells were fixed and subjected to immunostaining by antibodies for r-H2AX (Cell Signaling), FAK (Santa Cruz), or pMET (Cell Signaling), or the dyes F-actin (Alex 488, Life Technologies) or DAPI (Sigma-Aldrich) according to the Immunofluorescence General Protocol (https://www.cellsignal.com/contents/resources-protocols/immunofluorescence-general-protocol/if).

Statistical analysis

Student's *T*-test was used to determine statistical significance following the standard of a *p*-value less than 0.05–0.01. In the figures, * indicates a significant difference with $p < 0.05$, whereas ** indicates a significant difference with $p < 0.01$.

Phosphatase assay and enzyme activity analysis

The phosphatase enzyme assay was carried out using the substrates 5-bromo-4-chloro-3-indolyl phosphate–nitro blue tetrazolium (NBT/BCIP) and *para*-nitrophenyl phosphate (*p*NPP) (Life Technologies). The absorbance was measured at 590 nm for NBT/BCIP and 410 nm for *para*-nitrophenyl (*p*NP) (Bio Rad). *p*NP is a product of the *p*NPP substrate-catalyzed reaction. The ALP of calf-intestinal alkaline phosphatase (CIP, Life Technologies) was used as the positive control and vehicle water was used as the negative control for RP. Trypsin and α-amylase activities kits were purchased from Solarbio (Beijing, China). The methods are based on the protocols provided by the manufacturer.

Cell growth inhibition assay

For the two-dimensional cell growth assay, cells were treated with vehicle or agent. After 3–4 days, the cells were fixed and stained with crystal violet. Finally, a photograph was taken and the optical density was measured at 590 nm.

Fourier transform infrared (FT-IR) spectroscopy and quantitative measurement of elements

An FT-IR spectrometer (Nicolet iS5, resolution: 2 cm^{-1}) from Thermo Scientific was used to detect the chemical groups. The quantitative determination of sulfur in the samples was also carried out using Vario EL Cube elemental analyzer produced by Elementar (Germany). For each test, a 5 mg sample was accurately weighed on a balance with a precision of 0.001 mg and then wrapped in foil and put on a sample tray to be tested. The testing conditions of the elemental analyzer were as follows: combustion tube temperature 1150 °C, reduction tube temperature 850 °C, high-purity helium flow rate 220 mL min^{-1}, high-purity oxygen flow rate 50 mL min^{-1}, high-purity oxygen flow rate 80 s. After combustion, the samples were quantitatively analyzed by adsorption analytical column and thermal conductivity detector.

A Vario EL III elemental analyzer produced by Elementar (Germany) was used for the quantitative determination of hydrocarbon and nitrogen elements in the samples. Each test sample of 2–3 mg was accurately weighed on a balance with a precision of 0.001 mg and then wrapped in foil and put in a sample tray to be tested. The testing conditions of the elemental analyzer were as follows: combustion tube temperature 900 °C, reduction tube temperature 550 °C, high-purity helium flow 120 mL min^{-1}, high-purity oxygen flow 50 mL min^{-1}, high-purity oxygen flow of 30 s. After combustion, the samples were quantitatively detected by adsorption analytical column and thermal conductivity detector.

© 2021 The Author(s). Published by the Royal Society of Chemistry

Open Access Article. Published on 13 January 2021. Downloaded on 12/5/2025 2:40:49 AM.
This article is licensed under a Creative Commons Attribution-NonCommercial 3.0 Unported Licence.

Computational details

The ground state geometry of all possible isomers of the investigated molecules (*vide infra*) was fully optimized in aqueous solution at density-functional theory (DFT) using the M06-2X[48] hybrid functional coupled with the triple-ζ 6-311++G** (ref. 49 and 50) basis set. The absence of imaginary frequencies was checked for the optimized molecular geometries in harmonic approximation and the minima were found to be "genuine". Transition states for the phosphate transfer reaction were also optimized and the presence of one imaginary frequency was checked in the harmonic approximation. Thermochemical quantities were also calculated at $T = 298.15$ K and $p = 1$ atm for both minima and saddle points. Infrared intensities were also simulated for the points of minimum of the potential energy surface. Solvent effects were taken into account *via* the implicit polarizable continuum model in its integral equation formalism (IEF-PCM).[51] The PCM molecular cavity was built according to the SMD[52] parameterization. Standard values were always assumed for the dielectric constant and refractive index of water.

For all calculations for all the atomic species, the integration grid for the electronic density was set to 250 radial shells and 974 angular points. Accuracy for the two-electron integrals and their derivatives was set to 10^{-14} a.u. The convergence criteria for the self-consistent field method were set to 10^{-12} for the root mean square (RMS) change in the density matrix and 10^{-10} for the maximum change in the density matrix. Convergence criteria for the geometry optimizations were set to 2×10^{-6} a.u. for maximum force, 1×10^{-6} a.u. for RMS force, 6×10^{-6} a.u. for maximum displacement, and 4×10^{-6} a.u. for RMS displacement.

All calculations were performed using Gaussian G16.A03.[53]

Abbreviations

ALP	Alkaline phosphatase
TCM	Traditional Chinese medicine
Herbzyme	Herb enzyme
HR-AFM	High-resolution atomic-force microscopy
DFT	Density-functional theory
IEF-PCM	Polarizable continuum model in its integral equation formalism
NBT/BCIP	5-Bromo-4-chloro-3-indolyl phosphate–nitro blue tetrazolium
*p*NPP	*para*-Nitrophenyl phosphate
*p*NP	*para*-Nitrophenyl
FT-IR	Fourier transform infrared
SEM	Scan electron microscope
RP	Rhizoma polygonati
PL	Phosphatase-like

Author contributions

The manuscript was written by HF, with major revisions provided by EB and YX. Minor suggestions came from QS, QW, and AA, and some method parts from KD. The quantum mechanical calculations and the results analysis were performed by EB. Experiments were performed, designed or analyzed by the authors as follows: HF (chemistry), QS (SEM, element remeasurement, methods), KD (AFM), QW (herb processing), AS (enzyme and processing), AT (enzyme), LN (enzyme), AN (cell research), AK (enzyme and processing), CM (data), AD (enzyme and cell), MR (enzyme and cell), AK (enzyme), QY (cell), ZL (herb processing), XL (data), YX (cell research) either directly or indirectly through large-scale assistance with design and data analysis. XL and AA supervised the details in some experiments. YX led the project, such as, in concepts, designing, supervising, funding and more. KD fully carried out the HR-AFM scanning and analysis.

Funding

Nazarbayev University Faculty-Development Competitive Research Grants Program (ID: 15798117 *i.e.* ID: 16797152 (110119FD4531) to YX; and ID: 15874919 *i.e.* ID: 16796808 (110119FD4542) to HF and YX); United Arab Emirates University (UAEU)–Asian Universities Alliance (AUA) fellowship of 2019 (involving YX and AA).

Conflicts of interest

YX, HF, and QW disclose that the RP used in this work is a commercial patented RP product from Taian Xianlu Food Co Ltd and the company provided some reagents and funding to the project, in addition to the experimental contribution.

Acknowledgements

We thank the following for the support of the research. YX and HF thank the Nazarbayev University Faculty-Development Competitive Research Grants Program (ID 15798117 *i.e.* ID: 16797152 with title: Targeting cancer stem-like cells of castration-resistant prostate cancer through combinatorial inhibition of MET/nuclear MET and β-Catenin pathways: potential therapeutic intellectual property in prostate cancer treatment (110119FD4531) to YX and ID 15874919 *i.e.* ID: 16796808 with title: Phosphatase-like nanozyme activity of carbon nanodots and its potential as supplement for kinase inhibitor drug treating prostate cancer: potential intellectual property discovered in food product (110119FD4542) to HF and YX). YX thanks the United Arab Emirates University (UAEU)–Asian Universities Alliance (AUA) fellowship of 2019 (involving YX and AA). EB thanks Bingtuan Oasis research funding.

Notes and references

1 S. Li, *Compendium of Materia Medica (Bencao Gangmu)*, ed. L. Xiwen, Foreign Languages Press, Beijing, 2004.
2 P. Sionneau and B. Flaws, *Pao Zhi: An Introduction to the Use of Processed Chinese Medicinals*, Blue Poppy Pr, 1st edn, 1995.
3 M. D. Eisenberg, R. B. Davis, S. L. Ettner, S. Appel, S. Wilkey, M. Van Rompay and R. C. Kessler, Trends in alternative

Open Access Article. Published on 13 January 2021. Downloaded on 12/5/2025 2:40:49 AM.
This article is licensed under a Creative Commons Attribution-NonCommercial 3.0 Unported Licence.

medicine use in the United States. 1990–1997: results of a follow-up national survey, *JAMA, J. Am. Med. Assoc.*, 1998, **280**, 1569–1575.

4 D. Cyranoski, Why Chinese medicine is heading for clinics around the world, *Nature*, 2018, **561**, 448–450.

5 Y. Hu, S. Wang, X. Wu, J. Zhang, R. Chen, M. Chen and Y. Wang, Chinese herbal medicine-derived compounds for cancer therapy: a focus on hepatocellular carcinoma, *J. Ethnopharmacol.*, 2013, **149**, 601–612.

6 W. Lam, S. Bussom, F. Guan, Z. Jiang, W. Zhang, E. A. Gullen, S. H. Liu and Y. C. Cheng, The four-herb Chinese medicine PHY906 reduces chemotherapy-induced gastrointestinal toxicity, *Sci. Transl. Med.*, 2010, **2**, 45–59.

7 P. Zhao, C. Zhao, X. Li, Q. Gao, L. Huang, P. Xiao and W. Gao, The genus Polygonatum: a review of ethnopharmacology, phytochemistry and pharmacology, *J. Ethnopharmacol.*, 2014, **214**, 274–291.

8 T. Li, P. Wang, W. Guo, X. Huang, X. Tian, G. Wu, B. Xu, F. Li, C. Yan, X. J. Liang and H. Lei, Natural Berberine-Based Chinese Herb Medicine Assembled Nanostructures with Modified Antibacterial Application, *ACS Nano*, 2019, **13**, 6770–6781.

9 *WHO guidelines on good herbal processing practices for herbal medicines*, https://apps.who.int/medicinedocs/documents/s23449en/s23449en.pdf.

10 L. L. Chen, R. Verpoorte, H. R. Yen, W. H. Peng, Y. C. Cheng, J. Chao and L. H. Pao, Effects of processing adjuvants on traditional Chinese herbs, *J. Food Drug Anal.*, 2018, **26**, S96–S114.

11 X. Wu, S. Wang, J. Lu, Y. Jing, M. Li, J. Cao, B. Bian and C. Hu, Seeing the unseen of Chinese herbal medicine processing (Pao Zhi): advances in new perspectives, *Chin. Med.*, 2018, **17**(13), 4.

12 D. S. Kim, H. S. Kim, J. Lee, S. J. Hong, J. J. Cho, K. M. Cho and E. C. Shin, Comprehensive changes in volatile/nonvolatile compounds and flavor and physicochemical characteristics in Angelica gigas Nakai roots by thermal processing, *J. Food Biochem.*, 2019, **43**, e12842.

13 X. Su, Y. Wu, Y. Li, Y. Huang, Y. Liu, P. Luo and Z. Zhang, Effect of Different Post-Harvest Processing Methods on the Chemical Constituents of Notopterygium franchetii by an UHPLC-QTOF-MS-MS Metabolomics Approach, *Molecules*, 2019, **24**, 3188.

14 *Pharmacopoeia of the People's Republic of China English Edition*, The Stationery Office, London, 1st edn, 2017.

15 *Library of Chinese Humanities, the poetry of Du Fu*, ed. S. Owen, Walter de Gruyter Inc., Boston/Berlin, 2016, ch. 10, vol. 3, p. 34.

16 Note: "In TCM theory, *qi* is the vital substance constituting the human body. It also refers to the physiological functions of organs and meridians. There is no equivalent English word or phrase that completely describes the nature of *qi*. Most often, it is defined according to its functions and properties". For further readings, please refer to Shen Nong Shi http://www.shen-nong.com/eng/front/index.html.

17 S. Wilms, *Bei Ji Qian Jin Yao Fang: Essential Prescriptions Worth a Thousand in Gold for Every Emergency Chinese Medicine Database*, Bilingual edn, 2008.

18 L. Gao, J. Zhuang, L. Nie, J. Zhang, Y. Zhang, N. Gu, T. Wang, J. Feng, D. Yang, S. Perrett and X. Yan, Intrinsic peroxidase-like activity of ferromagnetic nanoparticles, *Nat. Nanotechnol.*, 2007, **2**, 577–583.

19 H. Sun, Y. Zhou, J. Ren and X. Qu, Carbon Nanozymes: Enzymatic Properties, Catalytic Mechanism, and Applications, *Angew. Chem., Int. Ed. Engl.*, 2018, **57**, 9224–9237.

20 B. J. Johnson, A. W. R. Algar, A. P. Malanoski, M. G. Ancona and I. L. Medintz, Understanding enzymatic acceleration at nanoparticle interfaces: approaches and challenges, *Nano Today*, 2014, **9**, 102–131.

21 X. X. Zheng, Q. Liu, C. Jing, Y. Li, D. Li, W. J. Luo, Y. Q. Wen, Y. He, Q. Huang, Y. T. Long, *et al.*, Catalytic gold nanoparticles for nanoplasmonic detection of DNA hybridization, *Angew. Chem., Int. Ed.*, 2011, **50**, 11994–11998.

22 Y. H. Hu, H. J. Cheng, X. Z. Zhao, J. J. Wu, F. Muhammad, S. C. Lin, J. He, L. Q. Zhou, C. P. Zhang, Y. Deng, *et al.*, Surface enhanced Raman scattering active gold nanoparticles with enzyme mimicking activities for measuring glucose and lactate in living tissues, *ACS Nano*, 2017, **11**, 5558–5566.

23 W. J. Luo, C. F. Zhu, S. Su, D. Li, Y. He, Q. Huang and C. H. Fan, Self-catalyzed, self-limiting growth of glucose oxidase-mimicking gold nanoparticles, *ACS Nano*, 2010, **4**, 7451–7458.

24 C. Xu and X. G. Qu, Cerium oxide nanoparticle: a remarkably versatile rare earth nanomaterial for biological applications, *NPG Asia Mater.*, 2014, **6**, e90.

25 A. J. Patil, R. K. Kumar, N. J. Barron and S. Mann, cerium oxide nanoparticle-mediated self-assembly of hybrid supramolecular hydrogels, *Chem. Commun.*, 2012, **48**, 7934–7936.

26 B. Garg and T. Bisht, Carbon nanodots as peroxidase nanozymes, *Molecules*, 2016, **21**, 1653.

27 W. Kang, J. Liu, J. Wang, Y. Nie, Z. Guo and J. Xia, Cascade biocatalysis by multienzyme-nanoparticle assemblies, *Bioconjugate Chem.*, 2014, **25**, 1387–1394.

28 P. Zhang, D. Sun, A. Cho, S. Weon, S. Lee, J. Lee, J. W. Han, D. P. Kim and W. Choi, Modified carbon nitride nanozyme as bifunctional glucose oxidase-peroxidase for metal-free bioinspired cascade photocatalysis, *Nat. Commun.*, 2019, **10**, 940–954.

29 A. A. Vernekar, D. Sinha, S. Srivastava, P. U. Paramasivam, P. D'Silva and G. Mugesh, Antioxidant nanozyme that uncovers the cytoprotective potential of vanadium nanowires, *Nat. Commun.*, 2014, **5**, 5301.

30 Y. Xie, H. Fan, W. Lu, Q. Yang, A. Nurkesh, T. Yeleussizov, A. Maipas, J. Lu, L. Manarbek, Z. Chen and E. Benassi, Nuclear MET requires ARF and is inhibited by carbon nanodots through binding to phospho-tyrosine in prostate cancer, *Oncogene*, 2019, **38**, 2967–2983.

31 S. Veeriah, C. Brennan, S. Meng, B. Singh, J. A. Fagin, D. B. Solit, P. B. Paty, D. Rohle, I. Vivanco, J. Chmielecki,

© 2021 The Author(s). Published by the Royal Society of Chemistry

Open Access Article. Published on 13 January 2021. Downloaded on 12/5/2025 2:40:49 AM.
This article is licensed under a Creative Commons Attribution-NonCommercial 3.0 Unported Licence.

W. Pao, M. Ladanyi, W. L. Gerald, L. Liau, T. C. Cloughesy, P. S. Mischel, C. Sander, B. Taylor, N. Schultz, J. Major, A. Heguy, F. Fang, I. K. Mellinghoff and T. A. Chan, The tyrosine phosphatase PTPRD acts a tumor suppressor frequently inactivating and mutating in glioblastoma and other human cancers, *Proc. Natl. Acad. Sci. U. S. A.*, 2009, **106**, 9435–9440.

32 Z. Wang, E. C. Southwick, M. Wang, S. Kar, K. S. Rosi, C. S. Wilcox, J. S. Lazo and B. I. Carr, The involvement of Cdc25A phosphatase in Hep3B hepatoma cell growth inhibition was found induced by the novel K vitamin analogs, *Cancer Res.*, 2001, **61**, 7211–7216.

33 J. Stebbing, L. C. Lit, H. Zhang, R. S. Darrington, O. Melaiu, B. Rudraraju and G. Giamas, The regulatory roles of phosphatases in cancer, *Oncogene*, 2014, **33**, 939–953.

34 C. M. Carbonaro, R. Corpino, M. Salis, F. Mocci, S. V. Thakkar, C. Olla and P. C. Ricci, On the emission properties of carbon dots: reviewing data and discussing models, *C*, 2019, **5**, 60.

35 A. Novogrodsky and J. Hurwitz, The enzymatic phosphorylation of ribonucleic acid and deoxyribonucleic acid. I. Phosphorylation at 5′-hydroxyl termini, *J. Biol. Chem.*, 1966, **241**, 2923–2932.

36 K. M. Holtz and E. R. Kantrowitz, The mechanism of the alkaline phosphatase reaction: insights from NMR, crystallography and site-specific mutagenesis, *FEBS Lett.*, 1999, **462**, 7–11.

37 J. G. Reinhild and G. A. Kfoury, Zinc-dependent enzymes in Zinc-depleted rats; intestinal alkaline phosphatase, *Am. J. Clin. Nutr.*, 1969, **22**, 1250–1263.

38 U. Sharma, D. Pal and R. Prasad, Alkaline Phosphatase: an overview, *Int. J. Clin. Biochem.*, 2014, **29**, 269–278.

39 X. Zhao and J. Li, Chemical constituents of the genus Polygonatum and their role in medicinal treatment, *Nat. Prod. Commun.*, 2015, **10**, 683–688.

40 *CRC Handbook of Chemistry and Physics*, ed. J. R. Rumble, CRC Press, Boca Raton, FL, 100th edn, 2010.

41 S. Feng, C. Bagia and G. Mpourmpakis, Determination of proton affinities and acidity constants of sugars, *J. Phys. Chem. A*, 2013, **117**, 5211–5219.

42 S. M. Rubin, Deciphering the retinoblastoma protein phosphorylation code, *Trends Biochem. Sci.*, 2013, **38**, 12–19.

43 X. Hu, L. Wu, Y. Wang, Y. Song, D. Mourant, R. Gunawan, M. Gholizadeh and C.-Z. Li, Acid-catalyzed conversion of mono- and poly-sugars into platform chemicals: effects of molecular structure of sugar substrate, *Bioresour. Technol.*, 2013, **133**, 469–474.

44 D. Mourant, Z. Wang, M. He, X. S. Wang, M. Garcia-Perez, K. Ling and C.-Z. Li, Yield and properties of bio-oil from the pyrolysis of mallee leaves in a fluidised bed reactor, *Fuel*, 2011, **90**, 2915–2922.

45 W. F. Wolkers, M. G. van Kilsdonk and F. A. Hoekstra, Dehydration-induced conformational changes of poly-L-lysine as influenced by drying rate and carbon hydrates, *Biochim. Biophys. Acta*, 1998, **1425**, 127–136.

46 K. Štefková, J. Procházková and J. Pacherník, Alkaline phosphatase in stem cells, *Stem Cells Int.*, 2015, **2015**, 628368.

47 X. Xiong, W. Peng, L. Chen, H. Liu, W. Huang, B. Yang, Y. Wang, Z. Xing, P. Gan and K. Nie, Traditional Chinese medicine Zhiqiao-Houpu herb-pair induce bidirectional effects on gastric motility in rats, *J. Ethnopharmacol.*, 2015, **175**, 444–450.

48 Y. Zhao and D. G. Truhlar, The M06 suite of density functionals for main group thermochemistry, thermochemical kinetics, noncovalent interactions, excited states, and transition elements: two new functionals and systematic testing of four M06-class functionals and 12 other functionals, *Theor. Chem. Acc.*, 2008, **120**, 215–241.

49 A. D. McLean and G. S. Chandler, Contracted Gaussian-basis sets for molecular calculations. 1. 2nd row atoms, Z=11-18, *J. Chem. Phys.*, 1980, **72**, 5639–5648.

50 K. Raghavachari, J. S. Binkley, R. Seeger and J. A. Pople, Self-Consistent Molecular Orbital Methods. 20. Basis set for correlated wave-functions, *J. Chem. Phys.*, 1980, **72**, 650–654.

51 J. Tomasi, B. Mennucci and R. Cammi, Quantum mechanical continuum solvation models, *Chem. Rev.*, 2005, **105**, 2999–3093.

52 A. V. Marenich, C. J. Cramer and D. G. Truhlar, Universal solvation model based on solute electron density and a continuum model of the solvent defined by the bulk dielectric constant and atomic surface tensions, *J. Phys. Chem. B*, 2009, **113**, 6378–6396.

53 M. J. Frisch, G. W. Trucks, H. B. Schlegel, G. E. Scuseria, M. A. Robb, J. R. Cheeseman, G. Scalmani, V. Barone, G. A. Petersson, H. Nakatsuji, *et al.*, *Gaussian 16, Rev. A.03*. Gaussian Inc., Wallingford CT, 2016.

© 2021 The Author(s). Published by the Royal Society of Chemistry